FEBS Letters

FEBS PRESS science publishing by scientists

# The PI 3-kinase PI3KC2α regulates mouse platelet membrane structure and function independently of membrane lipid composition

Maria V. Selvadurai[1], Rose J. Brazilek[1], Mitchell J. Moon[1], Jean-Yves Rinckel[2], Anita Eckly[2], Christian Gachet[2], Peter J. Meikle[3], Harshal H. Nandurkar[1], Warwick S. Nesbitt[1,4] and Justin R. Hamilton[1]

1 Australian Centre for Blood Diseases, Monash University, Melbourne, Australia
2 INSERM, EFS GEST, BPPS UMR_S1225, FMTS, Université de Strasbourg, France
3 Metabolomics Laboratory, Baker IDI Heart and Diabetes Institute, Melbourne, Australia
4 Microplatforms Research Group, School of Engineering, RMIT University, Melbourne, Australia

**Correspondence**
J. R. Hamilton, Australian Centre for Blood Diseases, Monash University, L1 AMREP Building, 99 Commercial Road, Melbourne, Vic. 3004, Australia
Fax: +61 3 9903 0228
Tel: +61 3 9903 0125
E-mail: justin.hamilton@monash.edu

(Received 31 October 2018, accepted 7 November 2018, available online 24 November 2018)

doi:10.1002/1873-3468.13295

Edited by Michael Bubb

**PI3KC2α is a phosphoinositide 3-kinase with a recently reported function in platelets; PI3KC2α-deficient mouse platelets have altered membrane structure and impaired function. Yet, how these membrane changes cause platelet dysfunction remains unknown. Here, focused ion beam-scanning electron microscopy of PI3KC2α-deficient platelet ultrastructure reveals a specific effect on the internal membrane structure, while liquid chromatography-tandem mass spectrometry profiling of 294 lipid species shows unaltered lipid composition. Functionally, PI3KC2α-deficient platelets exhibit impaired thrombosis specifically under conditions involving membrane tethering. These studies indicate that the structural changes in PI3KC2α-deficient platelets are limited to the membrane, occur without major changes in lipid composition, and selectively impair cell function during thrombus formation. These findings illustrate a unique mechanism that may be targetable for anti-thrombotic benefit.**

**Keywords:** open canalicular system; phosphoinositide 3-kinase; platelets; thrombosis

The phosphoinositide 3-kinases (PI3Ks) are a family of lipid kinases that catalyse the phosphorylation of the 3′ hydroxyl group of the inositol ring of phosphoinositides to produce the 3-phosphorylated phosphoinositides – important second messengers for a wide range of processes in cells [1,2]. There are eight mammalian PI3K isoforms, divided into three classes based on structural and functional similarities: four class I, three class II, and one class III PI3K. The class I PI3Ks are comfortably the most widely studied and have well-defined roles in range of cells, including platelets [3]. More recently, mouse genetic models have been used to uncover the importance of the sole class III PI3K, Vps34 [4,5], and one of the class II PI3Ks, PI3KC2α [6–8], in platelet function. PI3KC2α in particular regulates the thrombotic function of mouse platelets by a unique and as-yet-undefined mechanism that may involve the structure of the cell membrane. Specifically, we used an inducible shRNA-based approach to deplete PI3KC2α protein in the platelets of adult mice to show that PI3KC2α regulates the structure of the platelet internal membrane system (the

**Abbreviations**
FIB-SEM, focused ion beam-scanning electron microscopy; OCS, open canalicular system; PI3K, phosphoinositide 3-kinase; TEM, transmission electron microscopy.

open canalicular system; OCS) [6,7]. Here, transmission electron microscopy (TEM) revealed that PI3KC2α-deficient platelets exhibit dilatations of the channels of the OCS. Perhaps surprisingly, platelets from PI3KC2α-deficient mice displayed normal function in all *in vitro* function tests performed (aggregation, granule secretion, integrin activation, and adhesion and spreading on activating surfaces), yet have impaired platelet thrombotic function in both *in vitro* and *in vivo* models [6,7]. A subsequent study confirmed this role for PI3KC2α in platelet structure and function in a distinct mouse model involving heterozygosity of a kinase-inactivating point mutation in the PI3KC2α active site [8]. These intriguing findings suggest PI3KC2α links regulation of the platelet internal membrane structure to the cell's prothrombotic function. However, the mechanism by which this occurs remains unknown.

One potential mechanism by which alterations in the platelet membrane structure might impair platelet function is provided by the observation that PI3KC2α-deficient platelets exhibit reduced cytoskeletal co-localization of key proteins that link the cell membrane with the cytoskeleton, most notably spectrin and myosin [8]. If the reduction in these proteins is sufficient to impair communication between the membrane and cytoskeleton, one prediction is that this may lead to impaired filopodia formation in activated platelets. Yet how such an impact would result in the observed selective impairment of platelet function in the setting of thrombosis – and not a global impairment of platelet function in, for example, standard assays of aggregation, granule secretion, or platelet spreading [6], remains unclear.

Given this uncertainty regarding the mechanism by which PI3KC2α regulates platelet membrane structure and function, we have further examined the structural changes to the platelet membrane induced by PI3KC2α-deficiency and have investigated how these structural changes affect the function of the platelet membrane. Here, we use focused ion beam-scanning electron microscopy (FIB-SEM) [9], as well as traditional SEM, to perform a detailed, three-dimensional ultrastructural analysis of platelets from PI3KC2α-deficient mice. This analysis indicates PI3KC2α-deficient platelets exhibit specific changes to the structure of the OCS. These changes occur without major alterations in the lipid composition of these platelets. Surprisingly, the structural changes to the platelet OCS membrane have no impact on the formation of filopodia by platelets activated in suspension, yet markedly impacts on the ability of these platelets to form thrombi in a blood flow environment involving a prominent shear gradient that produces membrane tether formation [10–12]. Together, these findings indicate that PI3KC2α modulates the structure of the platelet internal membrane (OCS) independently of changes to membrane composition. These structural changes to the OCS appear to compromise platelet membrane function specifically in the setting of thrombus formation. If this regulation of membrane structure by PI3KC2α is acute, these studies reveal the potential for a novel approach toward thrombosis-specific anti-platelet therapy.

## Materials and methods

### Mice

All animal experiments were approved by the Alfred Medical Research and Education Precinct Animal Ethics Committee (approvals E/1465/2014/M and E/1644/2016/M). Mice were backcrossed ≥ 5 generations on a C57BL/6 genetic background (i.e. ≥ 98%) and maintained on a 12 h light/dark cycle with food and water *ad libitum*. All genetic studies were littermate controlled and were performed with mice at 6–20 weeks of age of either sex. Mice deficient in PI3KC2α (CMV-rtTA;TRE-GFP-shPI3KC2α) were generated using an inducible shRNA-based gene-silencing approach, as reported previously [6]. Control mice consisted of either pooled wild-type and monotransgenic littermates or were mice with similar transgenes but with a control shRNA targeting Renilla luciferase (CMV-rtTA; TRE-GFP-shControl). To induce shRNA-based knockdown of PI3KC2α expression, mice were placed on a doxycycline diet (600 $mg \cdot kg^{-1}$; Speciality Feeds, Glen Forrest, Australia), for at least 10 days prior to experimentation.

### Platelet isolation

Blood was drawn from the inferior vena cava of anaesthetized mice into enoxaparin (40 $U \cdot mL^{-1}$, final concentration), using a 25-gauge needle. Platelets were isolated as previously described [6]. Briefly, blood was treated with acid-citrate-dextrose and platelet wash buffer (4.3 mM $K_2HPO_4$, 4.3 mM $Na_2HPO_4$, 24.3 mM $NaH_2PO_4$, 113 mM NaCl, 5.5 mM D-glucose and 10 mM theophylline; pH 6.5; containing 0.5% BSA, 20 $U \cdot mL^{-1}$ enoxaparin and 0.01 $U \cdot mL^{-1}$ apyrase), platelets isolated *via* centrifugation, and resuspended in Tyrode's buffer containing 0.5% BSA, 1.8 mM $Ca^{2+}$ and 0.02 $U \cdot mL^{-1}$ apyrase.

### Focused ion beam-scanning electron microscopy

Isolated mouse platelets were fixed in 2.5% glutaraldehyde, postfixed in 1% osmium tetroxide and 1.5% potassium ferrocyanide, incubated in 4% uranyl acetate, and then

dehydrated through a series of graded ethanol concentrations before being embedded in Epon resin. Samples were imaged using a Helios NanoLab microscope (FEI, Tokyo, Japan). Stacks of approximately 1000 images with a field size of 15 μm × 15 μm were generated. Samples were milled with the FIB (20 kV) at a thickness of 20 nm per section. Three-dimensional models were computed using the imaging software AMIRA (FEI).

### Scanning electron microscopy

Isolated mouse platelets were activated with ADP under constant stirring in the presence of eptifibatide (40 $\mu g \cdot mL^{-1}$) and then fixed with the addition of glutaraldehyde (2.5%, final concentration). Fixed platelets were seeded on glass coverslips precoated with 0.01% poly-L-lysine; coverslips were then rinsed, dehydrated, and coated with a 10 nm layer of platinum/palladium or gold using a sputter coater (Cressington 208-HR; Cressington, Watford, UK). Imaging was performed, using a Nova NanoSEM 450 scanning electron microscope (FEI) at 5 kV, and analysis completed using FIJI software (open source).

### Platelet lipid composition

Platelet lipid composition analyses were performed as previously described [13,14]. Briefly, lipids were extracted using a single-phase chloroform : methanol extraction. Isolated mouse platelets in suspension were added to equal volumes of internal standard mix, comprising known concentrations of all lipid classes measured. A 2 : 1 ratio of chloroform : methanol was added to each sample. Samples were mixed with a rotary mixer for 10 min, sonicated for 30 min, and rested for 20 min at room temperature. Samples were then centrifuged at 16 000 ***g*** for 10 min and the resulting supernatant removed and dried with nitrogen gas at 40 °C. Samples were dissolved in water-saturated butanol and sonicated for 10 min prior to addition of an equal volume of methanol with 10 mM ammonium formate. The lipid extracts were centrifuged at 3350 ***g*** for 5 min and the supernatant removed for analysis.

Lipid analysis was performed using liquid chromatography electrospray ionization – tandem mass spectrometry, as previously described in detail [13,14], using an Agilent 1200 UHPLC coupled to an AB Sciex Q/TRAP 4000 mass spectrometer (SCIEX, Framingham, MA, USA) with a turboionspray source (350 °C) and Analyst 1.5 and Multiquant data systems (SCIEX). Separation by liquid chromatography was performed on a Zorbax C18 column (1.8 μm, 50 × 2.1 mm; Agilent Technologies, Santa Clara, CA, USA), again as previously described [13,14]. In total, 294 lipids were detected and quantitated.

The total lipid concentration for each class measured was determined by summing the concentrations of individual species in that class. Univariate comparisons were conducted comparing lipid classes between PI3KC2α-deficient (CMV-rtTA;TRE-GFP-shPI3KC2α) and littermate control mice, using Welch's *t*-test followed by Bonferroni correction to account for multiple comparisons.

### Microfluidic assay

Platelet aggregation was performed using a previously described method modified for use in this study with mouse whole blood [11]. Briefly, a microfluidic device consisting of 200 μm wide channels with inset 40 μm stenosis was fabricated using standard photolithography techniques [10]. Microchannels were selectively coated at the stenosis geometry with human vWF (10 $\mu g \cdot mL^{-1}$ – isolated from Biostate® CSL Ltd, Melbourne, Australia) for 10 min, blocked with BSA (2 $\mu g \cdot mL^{-1}$) for 10 min, then coated with botrocetin (2.5 $\mu g \cdot mL^{-1}$) for 10 min, before being flushed with Tyrode's buffer prior to sample perfusion. Hirudin-anticoagulated mouse whole blood was perfused through the microfluidic at 45 $\mu L \cdot min^{-1}$ (equating to a shear rate at the stenosis geometry of 11 500 $s^{-1}$) and platelet deposition at the stenosis monitored in real time *via* epifluorescence (Nikon Ti-U microscope – Plan Fluor 20×/0.50 (Nikon, Melville, NY, USA) objective with Andor Zyla sCMOS detector, Andor, Belfast, UK). Mid-plane platelet aggregate size was analysed in IMAGEJ (open source) following thresholding (Huang's fuzzy image thresholding method). Maximal aggregation, expressed as cross-sectional area ($\mu m^2$), was extrapolated from nonlinear curve fitting following 300 s perfusion time.

### Analyses

Statistical analyses were performed using GRAPHPAD PRISM (Graphpad, La Jolla, CA, USA). Statistical significance was defined at $P < 0.05$ and was determined with an unpaired, two-tailed Student's *t*-test, followed by Bonferroni correction to account for multiple comparisons where appropriate and as indicated in the figure legends.

## Results

### PI3KC2α regulates platelet membrane structure

We have previously used two-dimensional TEM imaging to demonstrate that PI3KC2α-deficiency results in a dilation of the channels of the OCS within mouse platelets [6]. In order to examine this and any other potential ultrastructural change caused by PI3KC2α-deficiency in more detail, we used FIB-SEM to create whole-cell, three-dimensional reconstructions of PI3KC2α-deficient mouse platelets. These reconstructions allow for visualization and quantitation of

various intracellular compartments, which in this case comprised the OCS and plasma membrane, as well as alpha and dense granules. In agreement with our previous two-dimensional findings, we observed dilation of the OCS in platelets from PI3KC2α-deficient mice when compared with platelets from littermate controls (Fig. 1A). Areas of OCS dilation in PI3KC2α-deficient platelets were more evident at certain points in a given cell (Fig. 1A, red arrows) and the total volume of OCS in platelets isolated from PI3KC2α-deficient mice was 48% greater than in platelets from littermate control mice (3.6 ± 0.5 vs 5.4 ± 0.6% of total cell volume for control and PI3KC2α-deficient cells, respectively; Fig. 1B). Despite this OCS dilation, no obvious differences were observed in the spatial distribution of the OCS throughout the cell (Fig. 1A). In contrast to the OCS, the total volume of either alpha or dense granules was not different between control and PI3KC2α-deficient platelets (Fig. 1C).

Given the OCS dilatation observed here and previously [6,7], we next examined the external aspect of the OCS – its openings at the plasma membrane – *via* SEM (Fig. 2A). There were similar numbers of OCS openings in the visible plasma membrane of cells examined in these studies (Fig. 2B). However, in a near-identical finding to the OCS measurements inside platelets, the diameter of OCS openings at the plasma membrane were significantly increased by 46% in platelets from PI3KC2α-deficient mice versus littermate controls (37 ± 4 vs 54 ± 3 nm, respectively; Fig. 2C).

## PI3KC2α does not regulate platelet membrane lipid composition

One of the most important contributors to membrane structure is the lipid content of the membrane. Therefore, we next examined whether the observed structural changes to the OCS were caused by or associated with alterations in the lipid profile of the platelet. We performed a detailed analysis of 294 lipids across the 22 most abundant lipid classes and subclasses, using liquid chromatography electrospray ionization-tandem mass spectrometry. This analysis revealed an unchanged lipid profile in PI3KC2α-deficient when compared with littermate control platelets (Fig. 3), with no significant differences in molar abundance observed in any of the lipid classes analysed.

## PI3KC2α does not regulate filopodia formation in platelets

We next examined whether the structural alteration in the platelet internal membrane impacts on platelet

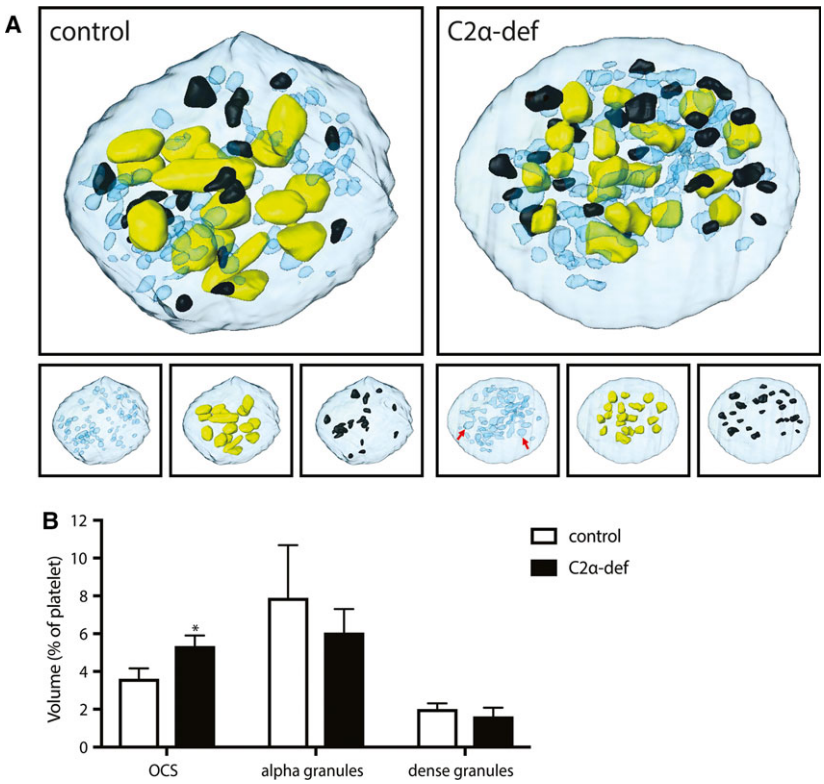


**Fig. 1.** PI3KC2α regulates internal platelet membrane structure. (A) Representative three-dimensional whole-cell FIB-SEM reconstructions of a platelet from a CMV-rtTA;TRE-GFP-shPI3KC2α bi-transgenic mouse (C2α-def) and a monotransgenic littermate (control) mouse, showing the OCS (blue), alpha granules (yellow), dense granules (black), and plasma membrane (light blue). Bottom panels show reconstructions with individual components only for clarity. Note dilation of the OCS in the PI3KC2α-deficient platelet (red arrows). (B) Quantitation of the volume of each organelle measured (as a percentage of the total platelet volume). Data are mean ± SEM from $n = 6$ platelets. *$P < 0.05$ (unpaired, two-tailed, Student's *t*-test).

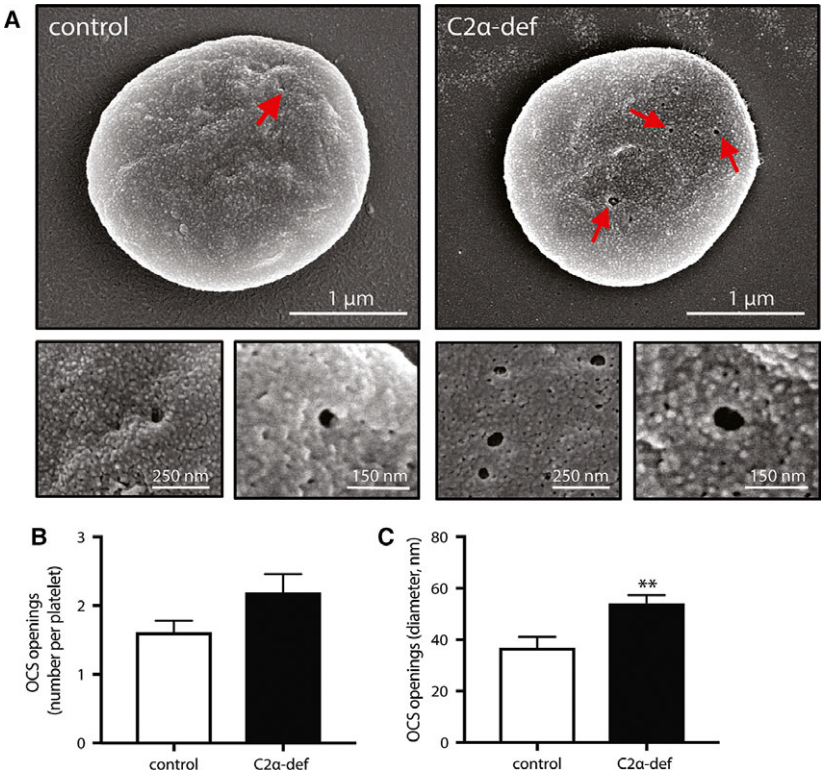


**Fig. 2.** PI3KC2α regulates external platelet membrane structure. (A) Representative SEM images of resting platelets isolated from CMV-rtTA;TRE-GFP-shPI3KC2α bitransgenic mice (C2α-def) or their wild-type and monotransgenic littermates (control), showing OCS surface openings (red arrows and the focus of the increased magnification images). (B) Number and (C) size of OCS openings. Data are mean ± SEM from $n = 112$ to 116 platelets from $n = 4$ mice per genotype. $^{**}P < 0.01$ (unpaired, two-tailed, Student's *t*-test).

membrane function by imaging filopodia formation in platelets activated in suspension or in the presence of shear forces. First, isolated platelets were stimulated with ADP (in the presence of eptifibatide to prevent aggregation), then fixed and imaged by SEM (Fig. 4A). No differences were detected in either the number or length of filopodia between platelets isolated from PI3KC2α-deficient or littermate control mice (Fig. 4B,C). In addition, filopodia formed by platelets flowed over a monolayer of activated platelets were also examined. Again, no differences in tether length or stability (total time of attachment) were observed (Fig. 4D,E).

### PI3KC2α regulates platelet adhesion and thrombus formation

Given the impaired arterial thrombus formation previously observed in PI3KC2α-deficient mice, we examined platelet function in a microfluidic whole blood flow assay known to be dependent on membrane tether formation [10–12]. Mouse blood was perfused through a von Willebrand factor-coated microfluidic channel incorporating a shear force gradient-inducing stenosis [10–12]. Platelet aggregation occurred downstream of the stenosis and the size of these platelet aggregates was quantified, using the epifluorescent signal of the GFP-positive platelets (Fig. 5). The extent of platelet deposition was significantly lower in blood from PI3KC2α-deficient mice (838 ± 314 $\mu m^2$) versus that in blood from control mice (2194 ± 485 $\mu m^2$) – a 62% reduction (Fig. 5).

Together, these findings suggest loss of PI3KC2α leads to a specific structural change in the platelet membrane that occurs independently of membrane lipid composition. This membrane modification is sufficient to selectively impact upon platelet function in the setting of thromboses formed downstream of a shear gradient-inducing stenosis and dependent on membrane tethering.

## Discussion

We performed an analysis of the structural and functional consequences of the loss of PI3KC2α in mouse platelets in order to gain insights into the mechanism by which PI3KC2α deficiency leads to the previously observed anti-thrombotic phenotype. We showed that PI3KC2α deficiency leads to an ultrastructural change in platelets that is limited to the internal membrane (OCS) of these cells. Specifically, the OCS in platelets from PI3KC2α-deficient mice was dilated throughout the cell, including at the plasma membrane. This structural change in the platelet membrane occurred

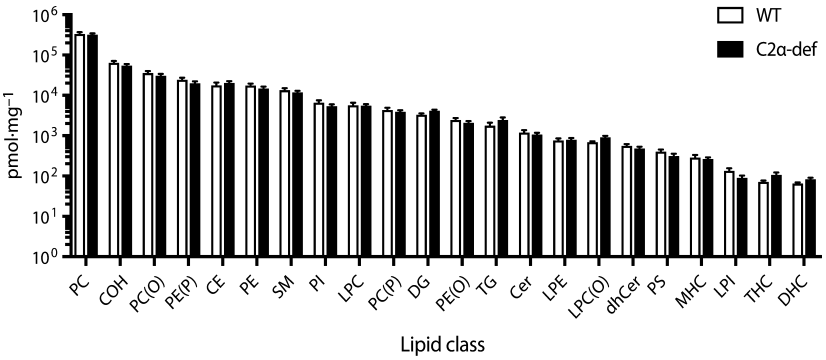


**Fig. 3.** PI3KC2α does not regulate platelet lipid composition. Concentration of the 22 most abundant lipid classes in platelets isolated from CMV-rtTA;TRE-GFP-shPI3KC2α bitransgenic mice (C2α-def) or their wild-type and monotransgenic littermates (control), *via* LC-ESI-MS/MS. Lipid classes are phosphatidylcholine (PC), free cholesterol (COH), alkylphosphatidylcholine (PC(O)), alkenylphosphatidylethanolamine (PE(P)), cholesterol ester (CE), phosphatidylethanolamine (PE), sphingomyelin (SM), phosphatidylinositol (PI), lysophosphatidylcholine (LPC), alkenylphosphatidylcholine (PC(P)), diacylglycerol (DG), alkylphosphatidylethanolamine (PE(O)), triacylglycerol (TG), ceramide (Cer), lysophosphatidylethanolamine (LPE), lysoalkylphosphatidylcholine (LPC(O)), dihydroceramide (dhCer), phosphatidylserine (PS), monohexosylceramide (MHC), lysophosphatidylinositol (LPI), trihexosylceramjde (THC) and dihexosylceramide (DHC). Molar abundance of each class is the total of the individual species within each class. Data are mean ± SEM from $n = 10$ to 13 mice per genotype. No significant differences were observed ($P > 0.05$ by unpaired, two-tailed, *t*-test with Bonferroni correction for multiple comparisons).

independently of the cell's lipid composition. Yet inspection of platelet membrane function revealed PI3KC2α deficiency had selective effects under prothrombotic conditions: filopodia formation was unaffected, but platelet deposition and aggregation was significantly impaired in an *ex vivo* whole blood flow thrombosis model.

We and others have previously shown that platelets from PI3KC2α-deficient mice exhibit an increased surface area occupied by the channels of the OCS in TEM images [6,8]. Here, we add to those findings to show that the enlargements previously reported in 2D TEM images are reflective of a widespread and largely uniform dilation of membrane channels throughout the cell, including at the plasma membrane. Our detailed three-dimensional analysis of PI3KC2α-deficient platelets revealed this structural change was specific to the OCS: its volume was significantly increased in PI3KC2α-deficient platelets while the volumes of alpha and dense granules were unaffected, despite the occasional change in granule number or shape between individual cells. Furthermore, the size of the openings of the OCS at the plasma membrane were significantly larger in PI3KC2α-deficient platelets. Despite this OCS dilation throughout the cell, no gross change in the spatial distribution of the OCS across the cell was observed.

Despite these obvious changes in the structure of the cell's membrane, it remains unclear how PI3KC2α-deficiency leads to such changes. It has previously been shown that PI3KC2α-deficiency reduces the basal levels of PI(3)P in platelets [8]. Yet, this small change in a low abundance lipid appears unlikely to directly cause the structural changes in the platelet membrane observed here. Given that the biggest predictor of any membrane structure is its lipid composition, here we expanded on these previous studies by performing a comprehensive analysis of the lipidome of both PI3KC2α-deficient and wild-type platelets. This more broad-based analysis included all of the most abundant membrane lipid species and revealed the gross lipid profile of PI3KC2α-deficient platelets was indistinguishable to that of wild-type platelets. These studies indicate the observed internal membrane dilatation is unlikely driven by compositional changes to the membrane. This is, to our knowledge, the most comprehensive lipidomic analysis of the mouse platelet. On this, it is interesting to note some potential differences in the relative abundance of some lipids between mouse platelets and similar lipidomic analyses of human platelets [15]. For example, while phospholipids are the predominant component in both mouse and human platelet membranes, there is a notably higher abundance of sterol lipids and a relative paucity of glycerolipids in mouse platelets when compared with human [15]. Whether these differences are important in terms of membrane function remains to be determined.

Previous studies have demonstrated an *in vivo* antithrombotic phenotype conferred by loss of PI3KC2α [6,8]. Given that platelets from these PI3KC2α-deficient mice have a structural defect that is specific to the OCS – a reserve of membrane thought to be utilized for platelet shape change and spreading

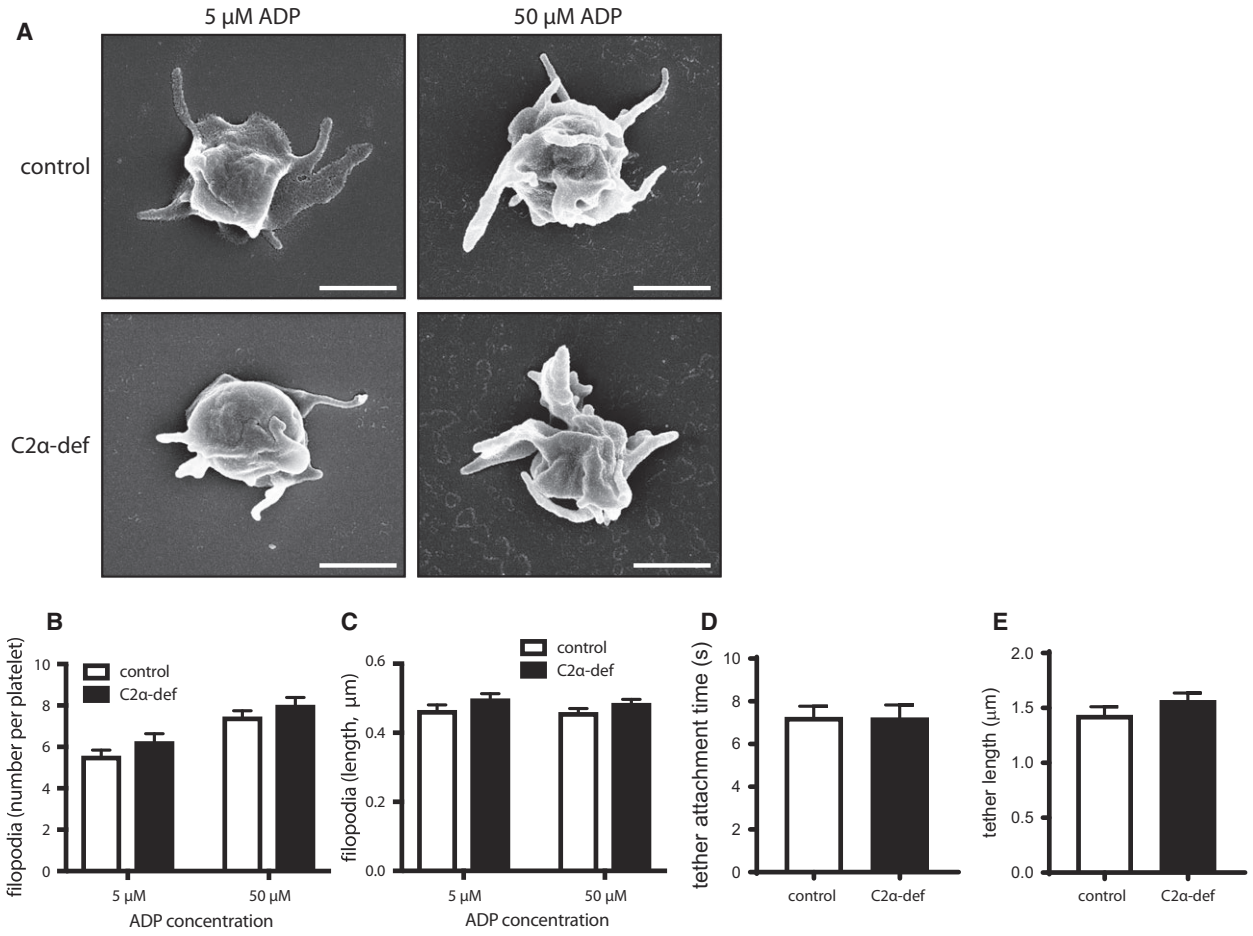


**Fig. 4.** PI3KC2α does not regulate filopodia formation. (A) Representative SEM images of platelets isolated from CMV-rtTA;TRE-GFP-shPI3KC2α bitransgenic mice (C2α-def) or monotransgenic littermates (control) and activated in suspension with 5 or 50 μM ADP (in the presence of eptifibatide to prevent aggregation). All scale bars are 1 μm. (B) Number and (C) length of filopodia per platelet. Data are mean ± SEM from $n = 119$ to 122 platelets from $n = 6$ mice per genotype. No significant differences were observed in any comparison ($P > 0.05$ by unpaired, two-tailed, *t*-test). (D) Length and (E) stability (total adhesion time) of filopodia from C2α-def or control platelets flowed over a monolayer of wild-type mouse platelets. Data are mean ± SEM from $n = 100$ platelets from $n = 5$ mice per genotype. No significant differences were observed in any comparison ($P > 0.05$ by unpaired, two-tailed, *t*-test).

during activation and aggregation [16] – we examined platelet membrane function in both static and blood flow environments. We found that platelet membrane function is affected specifically in the setting of thrombus formation. Here, filopodia production in suspension-activated platelets or under flow were unaffected by loss of PI3KC2α, yet in a microfluidic assay incorporating a high shear gradient-inducing stenosis, PI3KC2α-deficiency led to a marked reduction in platelet deposition. We utilized this microfluidic blood flow assay because of its incorporation of a pronounced stenosis that has been shown to cause a substantial shear gradient (from very high at the point of stenotic narrowing, to very low immediately downstream of the stenosis) [10–12]. Importantly, *in vivo* studies of platelet behaviour following exposure to such a shear gradient environment (*via* a vascular stenosis) have shown that initial platelet deposition occurs largely independently of cellular activation by soluble agonists [12]. Indeed, such shear gradients appear to drive initial platelet deposition via the formation of membrane tethers [10–12]. As a result, the significant reduction in platelet deposition in this system using blood from PI3KC2α mice may suggest that PI3KC2α is important for the earliest stages of platelet adhesion, where membrane tethers, presumably derived from the OCS, are pulled from platelets without detectable cell activation via an interaction between von Willebrand factor and the platelet adhesion receptor GPIbα [17]. This hypothesis fits our

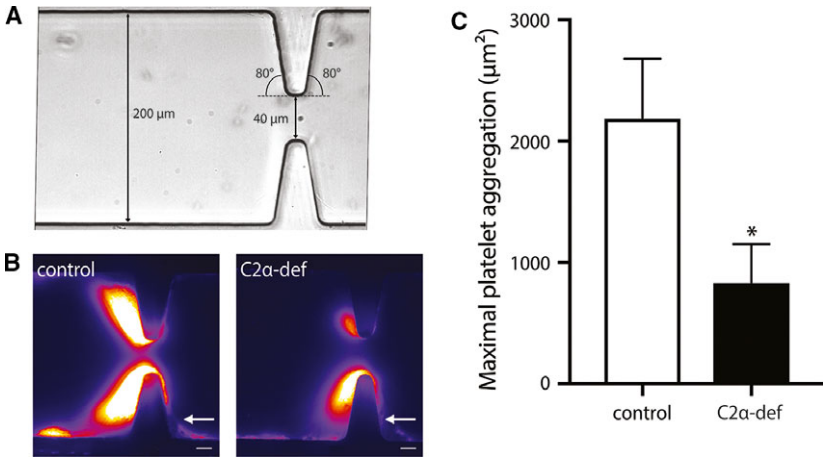


**Fig. 5.** PI3KC2α regulates platelet adhesion and deposition driven by a shear gradient. (A) DIC image showing the geometry of the microfluidic flow cell used in the whole blood flow assay. The channel has a width of 200 μm narrowing to 40 μm at the stenosis, with side-wall entry and exit angles of 80°. (B) Representative fluorescence images following perfusion of blood taken from CMV-rtTA;TRE-GFP-shPI3KC2α (C2α-def) or CMV-rtTA;TRE-GFP-shControl (control) mice through the flow cell shown in (A), with platelet aggregates seen forming downstream of the stenosis. Arrows indicate direction of flow. Scale bars, 10 μm. (C) Maximal platelet aggregation measured in these experiments (expressed as aggregate area). Data are mean ± SEM from $n = 5$ to 6 mice per genotype. $^*P < 0.05$ (unpaired, two-tailed, Student's *t*-test).

previous observations in which PI3KC2α-deficient platelet adhesion and thrombus formation is differentially affected under conditions in which platelet activation is substantial, that is, on a collagen-coated surface upon which marked platelet activation occurs [6]. Alternatively, PI3KC2α may be involved in the subsequent propagation of platelet aggregates, since incoming platelets that tether to the surface of forming thrombi are discoid and demonstrate low levels of activation markers and minimal calcium flux, in sharp contrast to the initial core of the thrombus where platelets are generally fully activated [12,18]. The lack of effect of PI3KC2α deficiency on platelet filopodia production in response to cell activation may suggest that the involvement of PI3KC2α is most prevalent where changes in shear stress sustain and drive thrombus propagation, potentially in the absence of conspicuous agonist-induced activation. The surprising lack of effect of PI3KC2α deficiency in standard assays of agonist-induced *in vitro* platelet function [6,8] supports this hypothesis.

The intriguing link between the PI3KC2α-dependent modulation of platelet internal membrane structure and impaired platelet function specifically in the setting of blood flow suggests targeting PI3KC2α and/or the platelet internal membrane system may have utility as an anti-thrombotic strategy. However, it remains unknown whether this function of PI3KC2α translates to human platelets. In addition, the relevance of changes in platelet membrane structure to human platelet function are completely unexplored. There are a number of clinical syndromes in which abnormalities in the OCS are observed, including some with either bleeding or thrombotic consequences [19–21]. Yet platelets from patients with these conditions demonstrate a number of structural abnormalities in addition to OCS changes, making it difficult to determine how much, if any, contribution the OCS defect has to the clinical phenotype. The development of PI3KC2α inhibitors would be a useful step forward in determining the role of this enzyme in human platelets and in addressing any validity of this target as an antithrombotic approach. If PI3KC2α function is conserved in human platelets and acute inhibition of this enzyme is able to reproduce the phenotype observed in mouse platelets, this opens the possibility of manipulating the platelet membrane structure *via* PI3KC2α as a novel, thrombosis-specific, antiplatelet strategy.

## Acknowledgements

Microfluidic devices were fabricated within the Micro Nano Research facility, RMIT University. We thank Monique Freund, Catherine Strassel, Fabienne Proamer and Neslihan Ulas for technical support; the staff of AMREP animal services for animal husbandry and care; staff of the Ramaciotti Centre for Cryo-Electron Microscopy and Monash Micro Imaging (Monash University) for assistance with microscopy; Jacqui Weir and Natalie Mellett for assistance with LC-MS;

and Andrew Yett for interesting insights. This work was supported by grants to JRH from the National Health Medical Research Council of Australia (1047295 and 1120522), Australian Research Council (FT130100540), and CASS Foundation (SM/16/7334).

## Author contributions

MVS performed research, analysed data and wrote the manuscript; RJB, MJM and J-YR performed research; AE, CG, PJM, HHN and WSN contributed to study design, data analysis and interpretation of results; JRH designed the study, interpreted results and wrote the manuscript.

## References

1 Jean S and Kiger AA (2014) Classes of phosphoinositide 3-kinases at a glance. *J Cell Sci* **127**, 923–928.
2 Vanhaesebroeck B, Stephens L and Hawkins P (2012) PI3K signalling: the path to discovery and understanding. *Nat Rev Mol Cell Biol* **13**, 195–203.
3 Valet C, Severin S, Chicanne G, Laurent PA, Gaits-Iacovoni F, Gratacap MP and Payrastre B (2016) The role of class I, II and III PI 3-kinases in platelet production and activation and their implication in thrombosis. *Adv Biol Regul* **61**, 33–41.
4 Valet C, Levade M, Chicanne G, Bilanges B, Cabou C, Viaud J, Gratacap MP, Gaits-Iacovoni F, Vanhaesebroeck B, Payrastre B *et al.* (2017) A dual role for the class III PI3K, Vps34, in platelet production and thrombus growth. *Blood* **130**, 2032–2042.
5 Liu Y, Hu M, Luo D, Yue M, Wang S, Chen X, Zhou Y, Wang Y, Cai Y, Hu X *et al.* (2017) Class III PI3K positively regulates platelet activation and thrombosis via PI(3)P-directed function of NADPH oxidase. *Arterioscler Thromb Vasc Biol* **37**, 2075–2086.
6 Mountford JK, Petitjean C, Putra HW, McCafferty JA, Setiabakti NM, Lee H, Tonnesen LL, McFadyen JD, Schoenwaelder SM, Eckly A *et al.* (2015) The class II PI 3-kinase, PI3KC2alpha, links platelet internal membrane structure to shear-dependent adhesive function. *Nat Commun* **6**, 6535.
7 Petitjean C, Setiabakti NM, Mountford JK, Arthur JF, Ellis S and Hamilton JR (2016) Combined deficiency of PI3KC2alpha and PI3KC2beta reveals a nonredundant role for PI3KC2alpha in regulating mouse platelet structure and thrombus stability. *Platelets* **27**, 402–409.
8 Valet C, Chicanne G, Severac C, Chaussade C, Whitehead MA, Cabou C, Gratacap MP, Gaits-Iacovoni F, Vanhaesebroeck B, Payrastre B *et al.* (2015) Essential role of class II PI3K-C2alpha in platelet membrane morphology. *Blood* **126**, 1128–1137.
9 Eckly A, Heijnen H, Pertuy F, Geerts W, Proamer F, Rinckel JY, Leon C, Lanza F and Gachet C (2014) Biogenesis of the demarcation membrane system (DMS) in megakaryocytes. *Blood* **123**, 921–930.
10 Tovar-Lopez FJ, Rosengarten G, Westein E, Khoshmanesh K, Jackson SP, Mitchell A and Nesbitt WS (2010) A microfluidics device to monitor platelet aggregation dynamics in response to strain rate micro-gradients in flowing blood. *Lab Chip* **10**, 291–302.
11 Brazilek RJ, Tovar-Lopez FJ, Wong AKT, Tran H, Davis AS, McFadyen JD, Kaplan Z, Chunilal S, Jackson SP, Nandurkar H *et al.* (2017) Application of a strain rate gradient microfluidic device to von Willebrand's disease screening. *Lab Chip* **17**, 2595–2608.
12 Nesbitt WS, Westein E, Tovar-Lopez FJ, Tolouei E, Mitchell A, Fu J, Carberry J, Fouras A and Jackson SP (2009) A shear gradient-dependent platelet aggregation mechanism drives thrombus formation. *Nat Med* **15**, 665–673.
13 Weir JM, Wong G, Barlow CK, Greeve MA, Kowalczyk A, Almasy L, Comuzzie AG, Mahaney MC, Jowett JB, Shaw J *et al.* (2013) Plasma lipid profiling in a large population-based cohort. *J Lipid Res* **54**, 2898–2908.
14 Giles C, Takechi R, Mellett NA, Meikle PJ, Dhaliwal S and Mamo JC (2016) The effects of long-term saturated fat enriched diets on the brain lipidome. *PLoS One* **11**, e0166964.
15 Slatter DA, Aldrovandi M, O'Connor A, Allen SM, Brasher CJ, Murphy RC, Mecklemann S, Ravi S, Darley-Usmar V and O'Donnell VB (2016) Mapping the human platelet lipidome reveals cytosolic phospholipase A2 as a regulator of mitochondrial bioenergetics during activation. *Cell Metab* **23**, 930–944.
16 Escolar G, Leistikow E and White JG (1989) The fate of the open canalicular system in surface and suspension-activated platelets. *Blood* **74**, 1983–1988.
17 Savage B, Saldivar E and Ruggeri ZM (1996) Initiation of platelet adhesion by arrest onto fibrinogen or translocation on von Willebrand factor. *Cell* **84**, 289–297.
18 Stalker TJ, Traxler EA, Wu J, Wannemacher KM, Cermignano SL, Voronov R, Diamond SL and Brass LF (2013) Hierarchical organization in the hemostatic response and its relationship to the platelet-signaling network. *Blood* **121**, 1875–1885.
19 Maldonado JE, Gilchrist GS, Brigden LP and Bowie EJ (1975) Ultrastructure of platelets in Bernard-Soulier syndrome. *Mayo Clin Proc* **50**, 402–406.
20 Dayal S, Pati HP, Pande GK, Sharma P and Saraya AK (1995) Platelet ultra-structure study in Budd-Chiari syndrome. *Eur J Haematol* **55**, 294–301.
21 White JG, Krumwiede MD and Escolar G (1999) Glycoprotein Ib is homogeneously distributed on external and internal membranes of resting platelets. *Am J Pathol* **155**, 2127–2134.